JOURNAL OF SOLID STATE CHEMISTRY **104,** 253–275 (1993)

The 1212 Superconductive Lead Cuprates: HREM Study

M. HERVIEU, T. ROUILLON, V. CAIGNAERT, AND B. RAVEAU

Laboratoire CRISMAT, ISMRA-Université de CAEN, Boulevard Maréchal Juin, 14050 Caen Cedex, France

Received June 1, 1992; in revised form October 5, 1992; accepted October 8, 1992

The 1212 lead cuprates, $Pb_{0.5}Sr_{2.5}Ca_{0.5}Y_{0.5}Cu_2O_{7-\delta}$ (superconductor) and $Pb_{0.7}Cu_{0.3}Sr_2Ca_{0.15}Y_{0.85}Cu_2O_{7-\delta}$ (nonsuperconductor), have been examined by electron microscopy. The E.D. patterns of both oxides are characterized by the existence of extra reflections, either incommensurate satellites or superstructures. The nature of the satellites is different in the two compounds. The HREM investigations of these phases show that the satellites observed in the E.D. patterns are mainly due to local order–disorder phenomena. For $Pb_{0.5}Sr_{2.5}Ca_{0.5}Y_{0.5}Cu_2O_{7-\delta}$, very large areas of the crystals exhibit a highly regular contrast; besides the regular distribution of the atoms, this phase shows very rare stacking faults, which have been interpreted, and modulated zones corresponding to a local ordering of the atoms of the perovskite layers. Finally one also observes, for this oxide, local superstructures corresponding to a modulation appearing in the (111) plane of the rock salt layer and interpreted as a local ordering of lead, oxygen, and vacancies. On the opposite the contrast of the nonsuperconducting phase, $Pb_{0.7}Cu_{0.3}Sr_2Y_{0.85}Ca_{0.15}Cu_2O_{7-\delta}$, is too disturbed to be interpreted, the most frequent feature being the speckled aspect of the crystals. These observations support the inhomogeneous character of the superconducting transition of the 1212 lead cuprates.

Introduction

The discovery of superconductivity up to 90 K in the oxide $Pb_{0.5}Sr_{0.5}Sr_2Y_{1-x}Ca_xCu_2O_{7-\delta}$ (*1*, *2*) has induced a systematic investigation of the superconducting properties of 1212 lead cuprates with the general formula $Pb_{1-y}A_ySr_2Y_{1-x}Ca_xCu_2O_{7-\delta}$ in which A = Ca (*3*), Cu (*4–11*), In (*12–15*), Cd (*16*, *17*), and other elements such as Mg, Zn, and Sc (*17*). The structural principles which characterize these phases were first established for the A = Sr superconductive cuprate (*1*) and for the nonsuperconductor $Pb_{0.7}Cu_{0.3}Sr_2Y_{0.85}Cu_{0.15}Cu_2O_{7-\delta}$ (*4*) almost simultaneously. They can be described as an intergrowth of double pyramidal copper layers, i.e., oxygen deficient perovskite layers, $[Sr(Ca, Y)_1Cu_2O_5]_\infty$, with double rock salt layers, $[SrPb_{1-x}A_xO_2]_\infty$ (Fig. 1), in agreement with the general formula $(ACuO_{3-\delta})_m(A'O)_n$ proposed at the beginning of the investigation of this large family of superconductive cuprates (*18*). Nevertheless, the single crystal diffraction (*5–7*) and powder neutron diffraction studies (*6*), if they all converge about the structure of the pyramidal copper layers, show significant differences and especially, in all cases, a strong disorganization of the rock salt layers at the level of the $[Pb_{1-y}A_yO]_\infty$ sheets. This high disorder of the lead–oxygen layers is of great importance, since it may be the origin of the inhomogenous character of superconductivity in these oxides, whose T_0 varies significantly with the nature of the A cations. In order to understand these phenomena, an electron microscopy study of these oxides was undertaken. We report here on two oxides with nominal compositions $Pb_{0.50}Sr_{0.50}Sr_2Y_{1-x}Ca_xO_{7-\delta}$ (x = 0.5 and 0) and $Pb_{1-y}Cu_ySr_2Y_{1-x}Ca_xO_{7-\delta}$ (x = 0.15, y = 0.3 and x = 0.5, y = 0.5).

0022-4596/93 $5.00

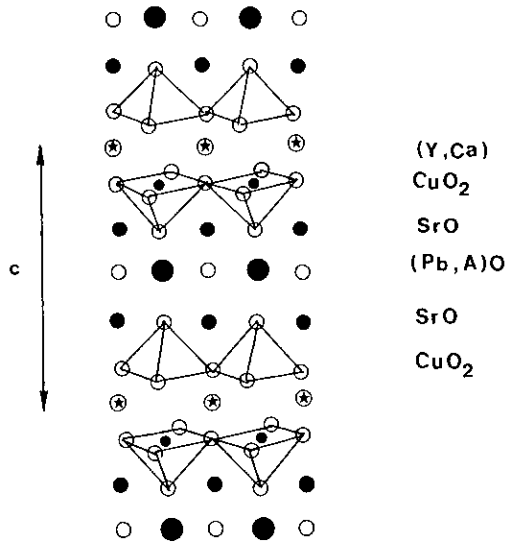

FIG. 1. Idealized drawing of the "1212" lead cuprate structure.

Experimental

Samples were prepared from mixtures of $PbO_2/PbO/Sr_2CuO_3/CuO/Y_2O_3$ and CaO in proportions corresponding to the nominal compositions $Pb_{0.5}Sr_{2.5}Y_{0.5}Ca_{0.5}Cu_2O_7$ and $Pb_{0.7}Sr_2Ca_{0.15}Y_{0.85}Cu_{2.3}O_7$. The oxides were intimately ground and pressed in the form of pellets. For the $Pb_{0.5}Cu_{0.5}Sr_2Ca_{0.5}Y_{0.5}Cu_2O_7$ sample, the pellets were sealed in quartz ampoules at 850°C for 6 hr and then cooled (0.3°C/min); $Pb_{0.7}Sr_2Y_{0.85}Ca_{0.15}Cu_{2.3}O_7$ was heated at 880°C in quartz tubes for 40 hr and then quenched (50°C/min).

The homogeneity of the samples was checked by X-ray diffraction. The powder X-ray diffraction patterns were registered by step scanning over an angular range of $10° \leq 2\theta \leq 120°$ in increments of 0.02° by means of a Philips diffractometer using Cu$K\alpha$ radiation. The X-ray diffraction patterns were used to refine the cell parameters and the crystal structure with the profile refinement computer program DBW 3.2.

The electron diffraction study was performed with a JEOL 120 CX electron microscope fitted with a side entry goniometer (±60°) and the HREM study with a JEM 200 CX fitted with a top entry goniometer (±10°) and an objective lens with $C_s = 0.8$ mm. High resolution image calculations were based on EMS program set (*19*).

Results and Discussion

Owing to the problems encountered in the structure determination of the lead 1212 cuprates by X-ray and neutron diffraction studies, a systematic investigation was performed by electron microscopy. Two samples of the different families were chosen, $(Pb_{0.5}Sr_{0.5})Sr_2(Y_{0.5}Ca_{0.5})Cu_2O_{7-\delta}$ and $(Pb_{0.7}Cu_{0.3})Sr_2(Y_{0.85}Ca_{0.15})Cu_2O_7$. The EDS analysis gave evidence of a strong difference in the Sr/Cu ratio, 1.15 and 0.9 respectively; these ratio are slightly different from the nominal ones (1.25 and 0.87) but in agreement with X.R.D. results which suggest a slight cation deficiency in the mixed intermediate layer. In the following section, the two samples are designated by their nominal compositions.

Electron Diffraction: Incommensurate Satellites and Superstructures

A great number of the investigated crystals show a lattice characteristic of the 1212 structure; i.e., one observes a set of intense reflections corresponding to the tetragonal cell with $a = b \approx a_p$ and $c \approx 11.9$ Å (a_p: parameter of the perovskite cubic cell). The impurities which were observed correspond for most of them to strontium carbonate. In most of the crystals one observes additional spots, but the "strontium cuprates" $Pb_{0.5}Sr_{0.5}Sr_2Y_{1-x}Ca_xCu_2O_{7-\delta}$ differ significantly from the "copper cuprates" $Pb_{0.7}Cu_{0.3}Sr_2Y_{1-x}Ca_xCu_2O_{7-\delta}$.

The oxides $Pb_{0.5}Sr_{0.5}Sr_2Y_{1-x}Ca_xCu_2O_{7-\delta}$. Most of the crystals exhibit additional spots corresponding either to incommensurate satellites or to diffuse streaks, whose intensity varies from one crystal to the other.

Satellites are observed in the [100] and [010] E.D. patterns both for the $x = 0.50$

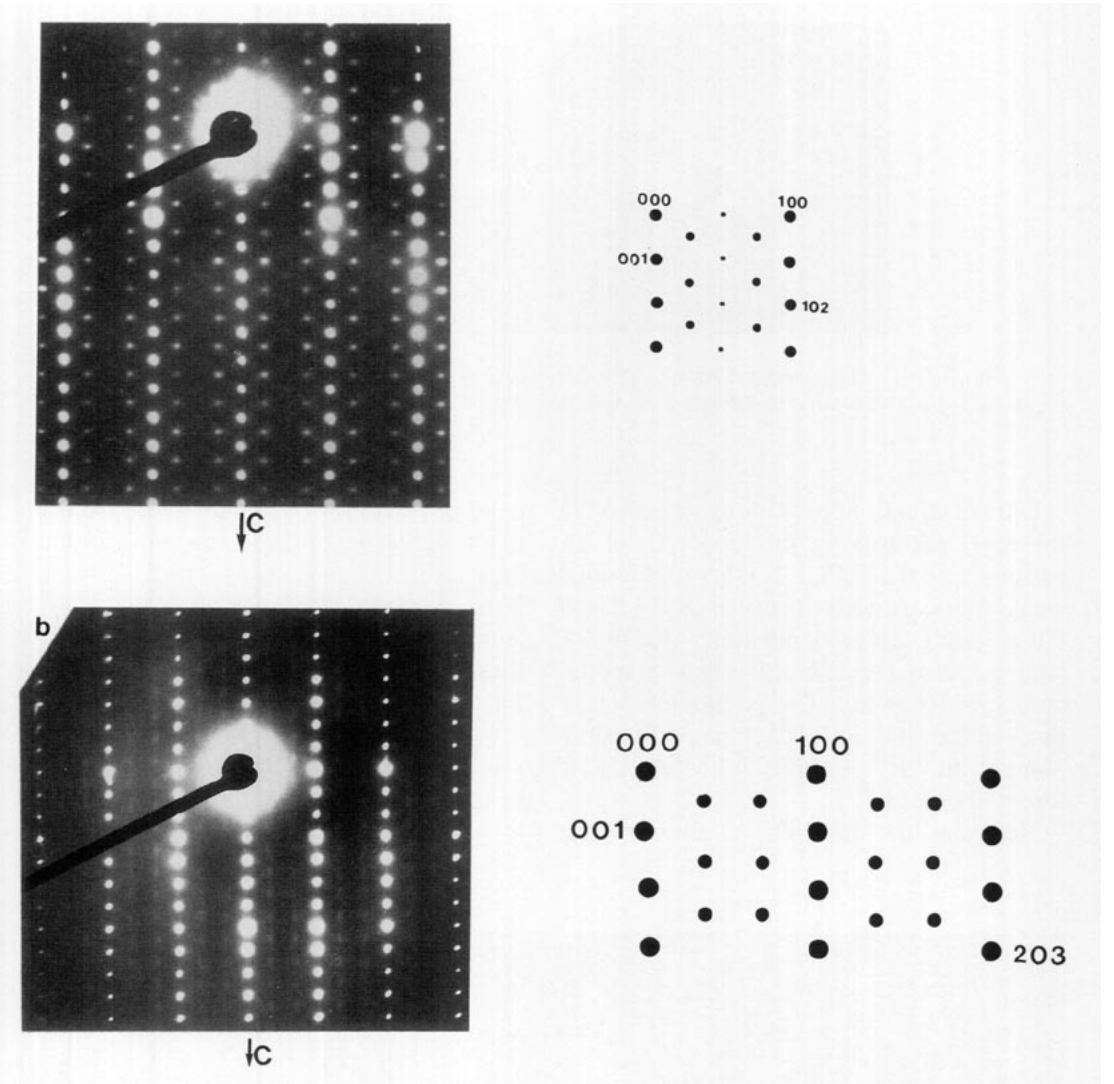

FIG. 2. [010] E.D. pattrens observed in $Pb_{0.5}Sr_{2.5}Y_{0.5}Ca_{0.5}Cu_2O_{7-\delta}$. a) Satellites along [102]* with $q \sim 4$ and b) satellite along [203]* with $q \sim 6$.

superconductor and for the insulating phase corresponding to $x = 0$. Two examples of [010] E.D. patterns are shown in Fig. 2 for the phase $x = 0.50$ which exhibit satellites with a modulation vector q close to 4 (Fig. 2a) and 6 (Fig. 2b) along the directions [102]* and [203]*, respectively. The satellites are very intense in the first case, whereas they are weak in the second case; similar satellites are observed for $x = 0$ in the [010] pattern with a q vector to 4 along [102]* but with weaker intensity. The $x = 0$ phase differs from $x = 0.50$ by the existence of satellites in the [001] E.D. pattern which exhibit a great variety in the directions they lie along; two examples are shown. The first one, Fig. 3a, corresponds to a direction [210]* with a q vector close to 5. The second corresponds to a superstructure "$a_p\sqrt{2} \times a_p\sqrt{2}$," superposed on a modulation along the [710]* direction, also often observed.

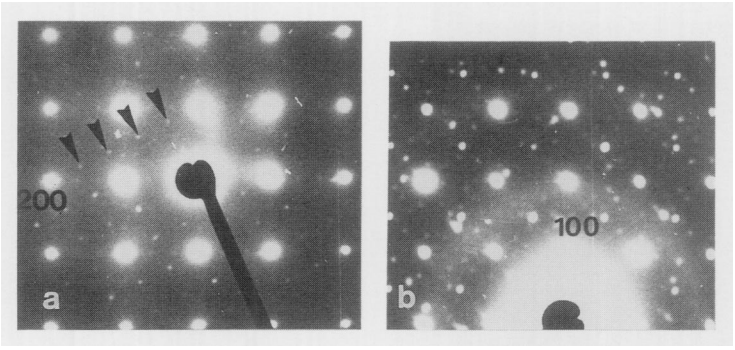

FIG. 3. [001] E.D. patterns of $Pb_{0.5}Sr_{2.5}YCu_2O_7$ a) satellites along [210]* with $q \sim 5$ b) a superstructure $a_p\sqrt{2} \times a_p\sqrt{2}$ is superposed with a modulation along [710]*.

Diffuse streaks appear along a^* and b^* in the [001] patterns as shown for the E.D. pattern $x = 0.50$ (Fig. 4) where additional weak spots are also observed in $0\ \frac{1}{2}\ 0$ and $\frac{1}{2}\ 0\ 0$ (white arrows) positions. From the latter pattern, it appears clear that the modulations which induce this phenomenon take place in the (100) or (010) plane, with a doubling of the "a" or "b" parameters, in 90° oriented domains.

Note that the annealing of these oxides in an oxygen flow at low temperature leads to a progressive disappearance of the satellites.

The oxides $Pb_{1-y}Cu_ySr_2Y_{1-x}Ca_xCu_2O_{7-\delta}$. Additional reflections are also observed for these oxides but of a different kind than for $Pb_{0.5}Sr_{0.5}Sr_2Y_{1-x}Ca_xCu_2O_{7-\delta}$.

For $Pb_{0.5}Sr_2Y_{0.5}Ca_{0.5}Cu_{2.5}O_{7-\delta}$, the diffuse streaks in the [001] patterns have disappeared and are replaced by superstructures as shown for instance in Fig. 5, where a

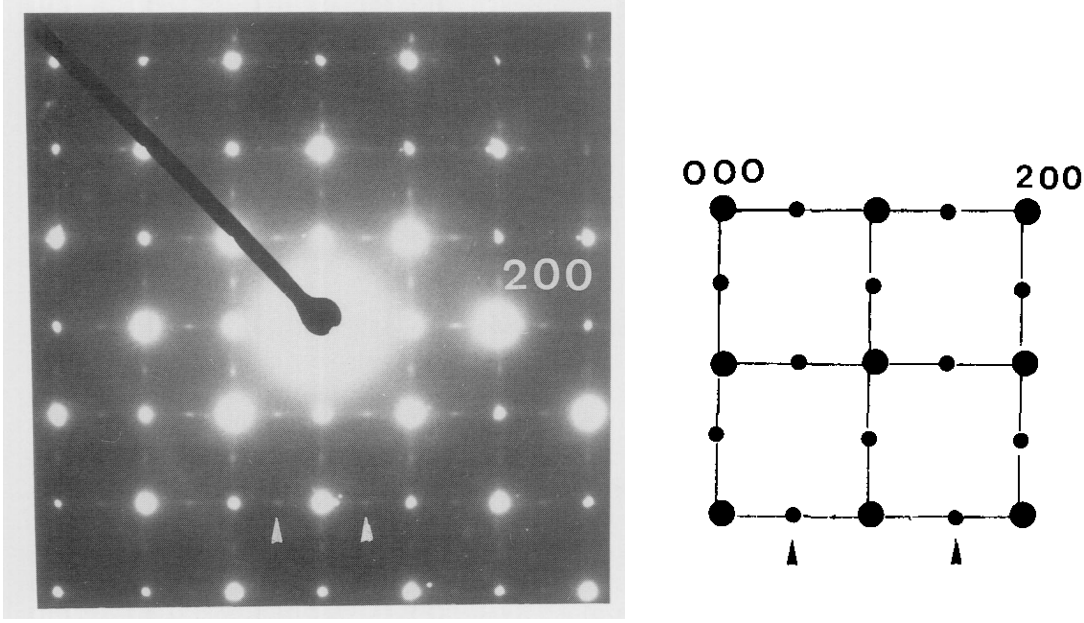

FIG. 4. [001] E.D. of $Pb_{0.5}Sr_{2.5}Y_{0.5}Ca_{0.5}Cu_2O_{7-\delta}$ where diffuse streaks are observed.

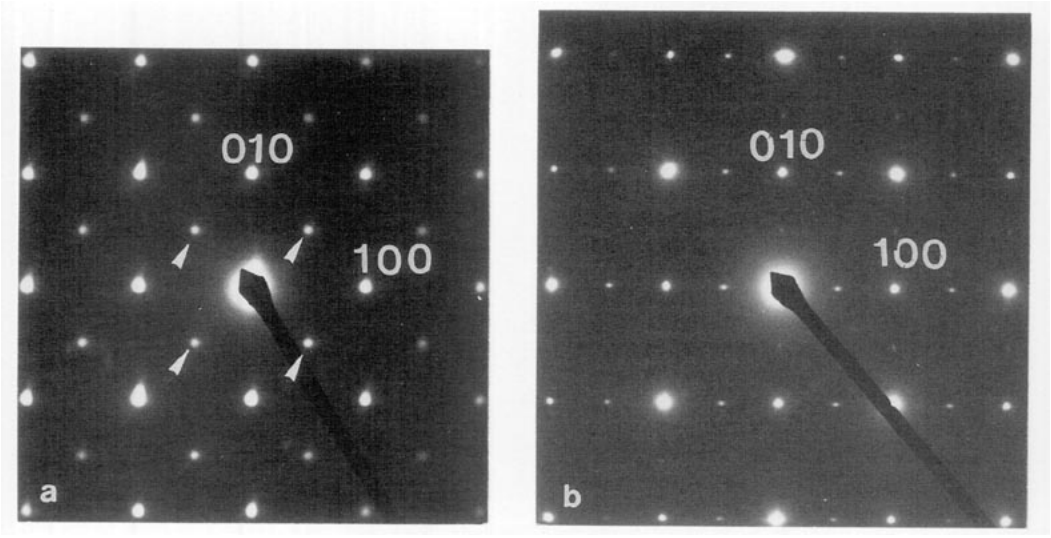

FIG. 5. $Pb_{0.5}Sr_2Y_{0.5}Ca_{0.5}Cu_{2.5}O_{7-\delta}$: [001] E.D. patterns with a) $a_p\sqrt{2} \times a_p\sqrt{2}$ (additional spots are shown by white triangles) and b) $2a_p \times a_p$ superstructures.

weak orthorhombic distortion is clearly visible (white arrows).

For $Pb_{0.7}Sr_2Y_{0.85}Ca_{0.15}Cu_{2.3}O_{7-\delta}$, different phenomena are observed in the [001] E.D. pattern planes. Indeed strong variations of the intensity of the h k 0 fundamental reflections are observed for $h + k = 2n + 1$, as shown in Fig. 6, where it can be seen that in some crystals the "$h + k = 2n + 1$" reflections are as intense as the "$h + k = 2n$" reflections, (Fig. 6a), whereas in others they are very weak (Fig. 6b). Moreover numerous [001] E.D. patterns exhibit satellites along $[1\bar{1}0]^*$ and $[100]^*$ as shown in Fig. 7. Such satellites can appear in commensurate position along

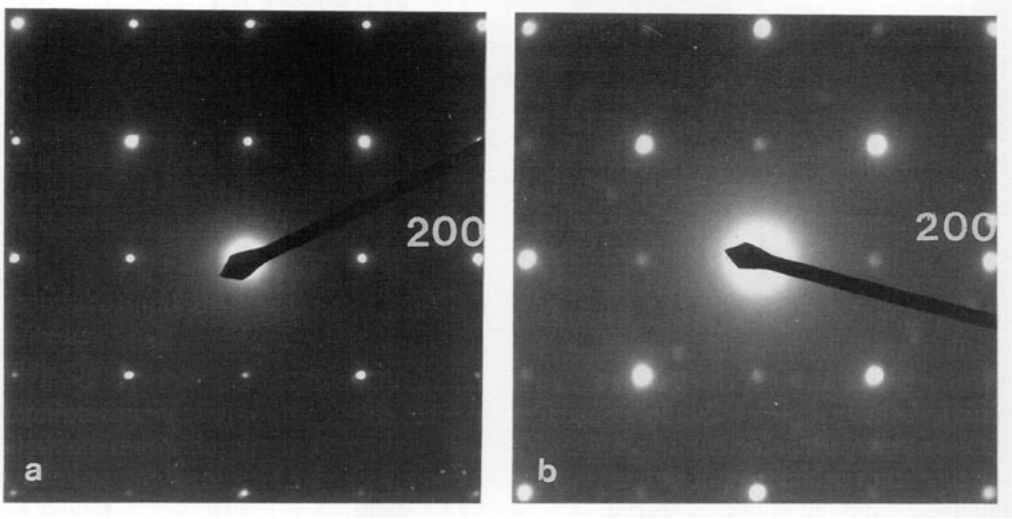

FIG. 6. $Pb_{0.7}Sr_2Y_{0.85}Ca_{0.15}Cu_{2.3}O_{7-\delta}$: the $h + k = 2n$ reflections can be strong (a) or very weak (b) in the [001] E.D. pattern.

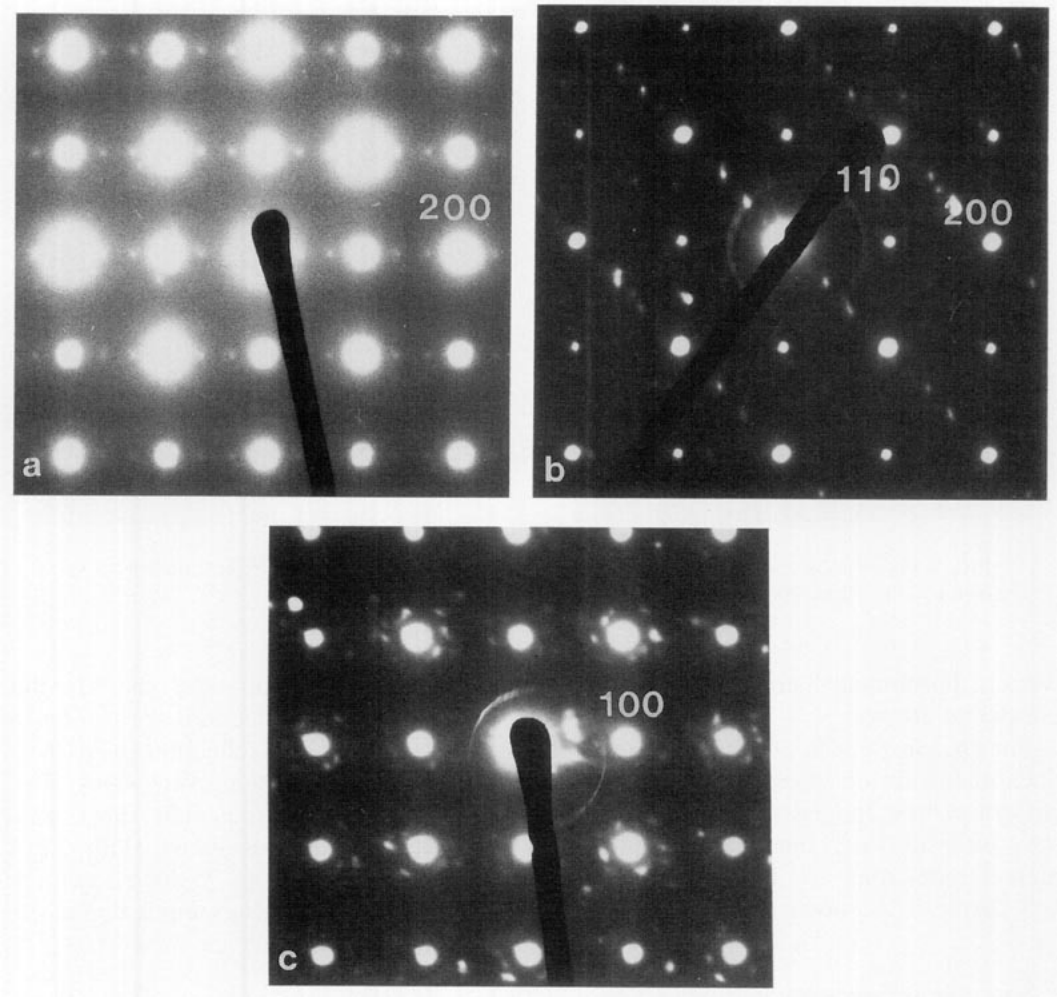

FIG. 7. $Pb_{0.7}Sr_2Y_{0.85}Ca_{0.15}Cu_{2.3}O_{7-\delta}$ = a) extra reflections involving a tripling of the parameter are observed b) Others, lying in incommensurate position along $[1\bar{1}0]^*$ are also observed, with $q \sim 2.67$. c) more complex systems are sometimes observed. In that example, two sets of modulations are superposed.

a^* with a periodicity $a' \approx 3a_p$, $b' \approx a_p$ (Fig. 7a). They can also appear along $[1\bar{1}0]^*$ (Fig. 7b) on one row out of two, suggesting two sets of lattices, one "$a_p \times a_p$" lattice and one lattice similar to that of Fig. 6b, i.e., modulated along $[1\bar{1}0]^*$ with $q \approx 2.67$. More complex E.D. patterns are sometimes observed, which can be interpreted as the superposition of two (or more) sets of modulations (one example is shown in Fig. 7c).

It is worth pointing out that in the [100] E.D. patterns the satellites are weak for $x = 0.15$ and in position $0\ \frac{1}{3}\ \frac{1}{2}$, whereas they are absent for $x = 0.50$, in contrast to the "$Pb_{0.5}Sr_{0.5}$" oxides, which exhibit intense satellites.

These satellites suggest order–disorder phenomena, taking into account the existence of cations of different sizes in the same $[Pb_{1-y}A_yO]_\infty$ layer, the possible Sr–Y substitution, and also a possible variation of oxygen stoichiometry. In order to understand these phenomena, an HREM study was performed on two oxides with different cationic

compositions in the rock salt layers, $Pb_{0.5}Sr_{0.5}Sr_2Ca_{0.5}Y_{0.5}Cu_2O_{7-\delta}$ and $Pb_{0.7}Cu_{0.3}Sr_2Cu_{0.15}Y_{0.85}Cu_2O_{7-\delta}$.

HREM Study

The complexity of the 1212-type lead cuprates, especially the nature of the $[Pb_{1-x}A_xO]_\infty$ intermediate layer which was not entirely solved by X-ray and neutron diffraction, raises the question of the limits of the HREM technique for such an issue. In order to interpret the image contrast at the level of the mixed rock salt layer containing lead (labelled P), we have performed image calculations based on two types of structural hypotheses: the cations Pb/Sr/Cu are statistically distributed over the atomic sites of the layer "P" or they are segregated in different types of layers or domains, aleatorily distributed over the matrix so that they cannot be refined by X-ray and neutron diffraction techniques.

A first series of simulated images (Fig. 8) was then calculated on the basis of statistical occupation of "P" by the different possible cations, keeping constant the atomic positions obtained from X-ray and neutron diffraction refinements. Various hypotheses of cation distribution were considered, $[Pb_{0.5}Sr_{0.35}]$, $[Pb_{0.5}Cu_{0.46}]$, or $[Pb_{0.66}\square_{0.3}]$, which take into account the cation deficiency observed at that site by diffraction techniques. It appears clearly from the calculated images that the different distributions do not give rise to significant variations of the contrast, so that they would not be detected in the experimental images (Figure 8a). If we consider extreme distributions with P layers occupied only by Sr or Cu, it appears that the small variations of contrast are also scarcely detectable (Fig. 8b and c, respectively). A second series of simulated images was calculated, taking into consideration a possible coexistence of two or three types of layers in the matrix, $[Pb_{1-y}O]$, $[SrO]_\infty$, and $[CuO_x]_\infty$; these different layers could be aleatorily stacked along the **c** axis or distributed in domains in a mosaic-type structure. The two first types of layers are rock salt-type layers and the third one a perovskite layer. For such an assumption, one must take into account the interatomic distances usually observed in these structural types and so, consider a variation of the c parameter. Some calculated images for such structural hypotheses are shown in Fig. 9 and can be compared with the first series of images. In that case, we observe indeed a significant variation of the contrast which could be experimentally detected. These results are of importance since they show that no significant variation of the contrast could be detected by HREM for the variations of the cation content corresponding to the possible extreme distributions between Pb/Sr/Cu and vacancies if the environment, and especially the adjacent $[SrO]_\infty$ layers, are not modified by the cation substitution. On the contrary, any variation which involved such a modification of the environment would be detected easily by the interlayer distances and a contrast variation.

$Pb_{0.5}Sr_{0.5}Sr_2Ca_{0.5}Y_{0.5}Cu_2O_{7-\delta}$

For the sample corresponding to the nominal composition $Pb_{0.5}Sr_{0.5}Sr_2Ca_{0.5}Y_{0.5}Cu_2O_{7-\delta}$, we focused our attention on four points dealing with the contrast at the level of the layer P, the layer stacking, the contrast associated with the existence of satellites in E.D. patterns, and the characterization of local phenomena.

Contrast at the level of the layers P. From examination of numerous crystals which exhibit E.D. patterns without satellites, a highly regular contrast is observed. No significant variation of the contrast and no variation in the interlayer distances were detected from one layer to an adjacent one, any more than along the layer. The study of the experimental through focus images shows that they fit well with the images calculated for the refined atomic positions. An overall image is shown in Fig. 10a and the comparison between calculated and experimental images is shown in Fig. 10b. For Δf close to -400 Å the bright zones are

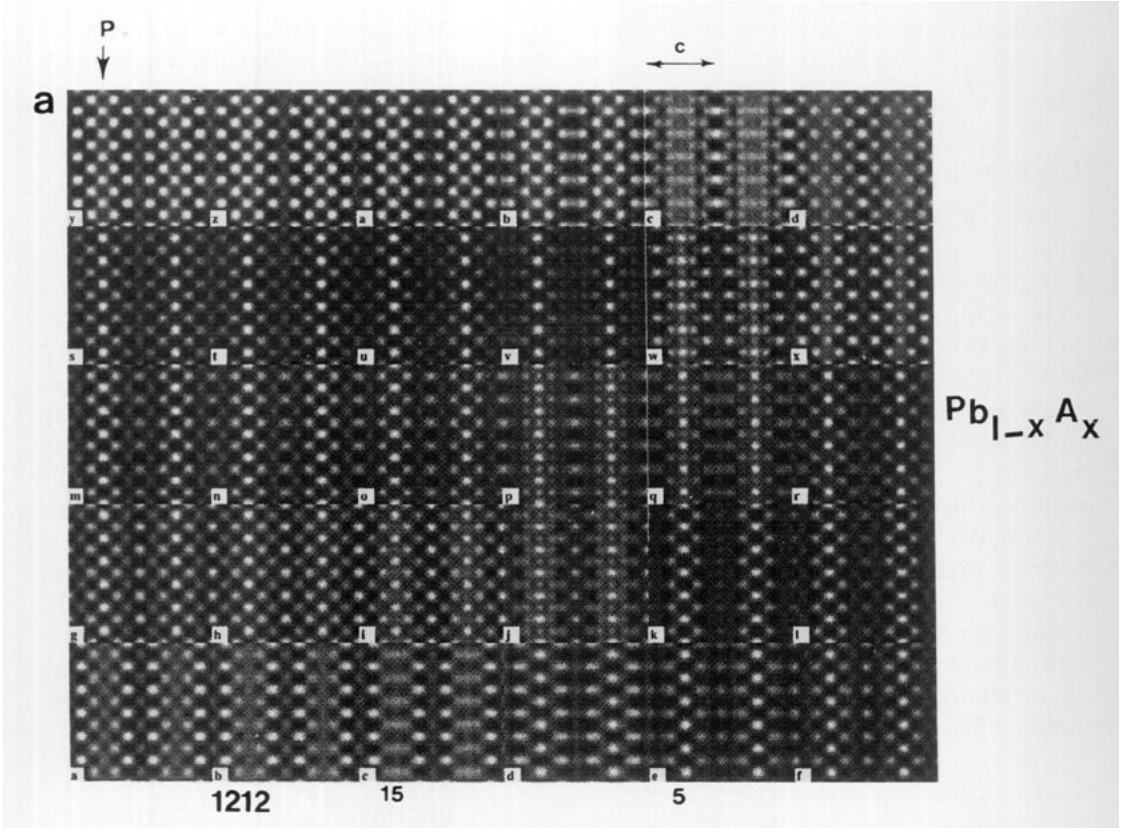

FIG. 8. Through focus calculated images for different cation distributions and based on the atomic positions determined by X-ray and neutron diffraction calculations. a) $(Pb_{1-x}A_x)Sr_2Y_{0.5}Ca_{0.5}Cu_2O_{7-\delta}$, A = Sr, Cu or ❑; b) (Sr) $Sr_2Y_{0.5}Ca_{0.5}Cu_2O_{7-\delta}$; c) (Cu) $Sr_2Y_{0.5}Ca_{0.5}Cu_2O_{7-\delta}$. The images are calculated from 25 to −120 nm (every 5 nm), the thickness is 3.1 nm.

correlated to the low electronic density zones, the brightest rows corresponding to the layers "P." For Δf close to −700 Å, the zones of high electronic density are highlighted, the layers P being the brightest ones. Two other images are shown, where the $[Y, Ca]_\infty$ row is well imaged: for Δf close to −950 Å, it appears as a dark row, whereas for $\Delta f \sim -1200$ Å it appears as a bright row.

It must be emphasized that these zones of regular contrast correspond, by far, to very large areas of the crystals.

The layer stacking. In the same way the stacking of the layers according to a 1212 mode can be considered as almost perfect (Fig. 10a). Very few intergrowth defects were observed; three examples of defects are given in Figs. 11 to 13 since the involved structural mechanism is of interest. The first type of defect in the layers stacking is presented in Fig. 11a where the bright dots are correlated with the positions of lead and strontium atoms. At the level of the defect (curved arrow) two rows of bright dots, correlated with "P" layers, sandwich two layers of weak contrast, in staggered rows. The interlayer distances, close to 5.3 Å, suggests the formation of rock salt-type layers and the weak contrast suggests the absence of lead in these intercalated layers. The new sequence is then $[SrO]_\infty$ $[P]_\infty$ $[(Sr, Ca)_1O]_\infty$ $[(Sr, Ca)_1O]_\infty$ $[P]_\infty$ $[SrO]_\infty$, leading to the formation of a defective member $n' = 5$ (Fig.

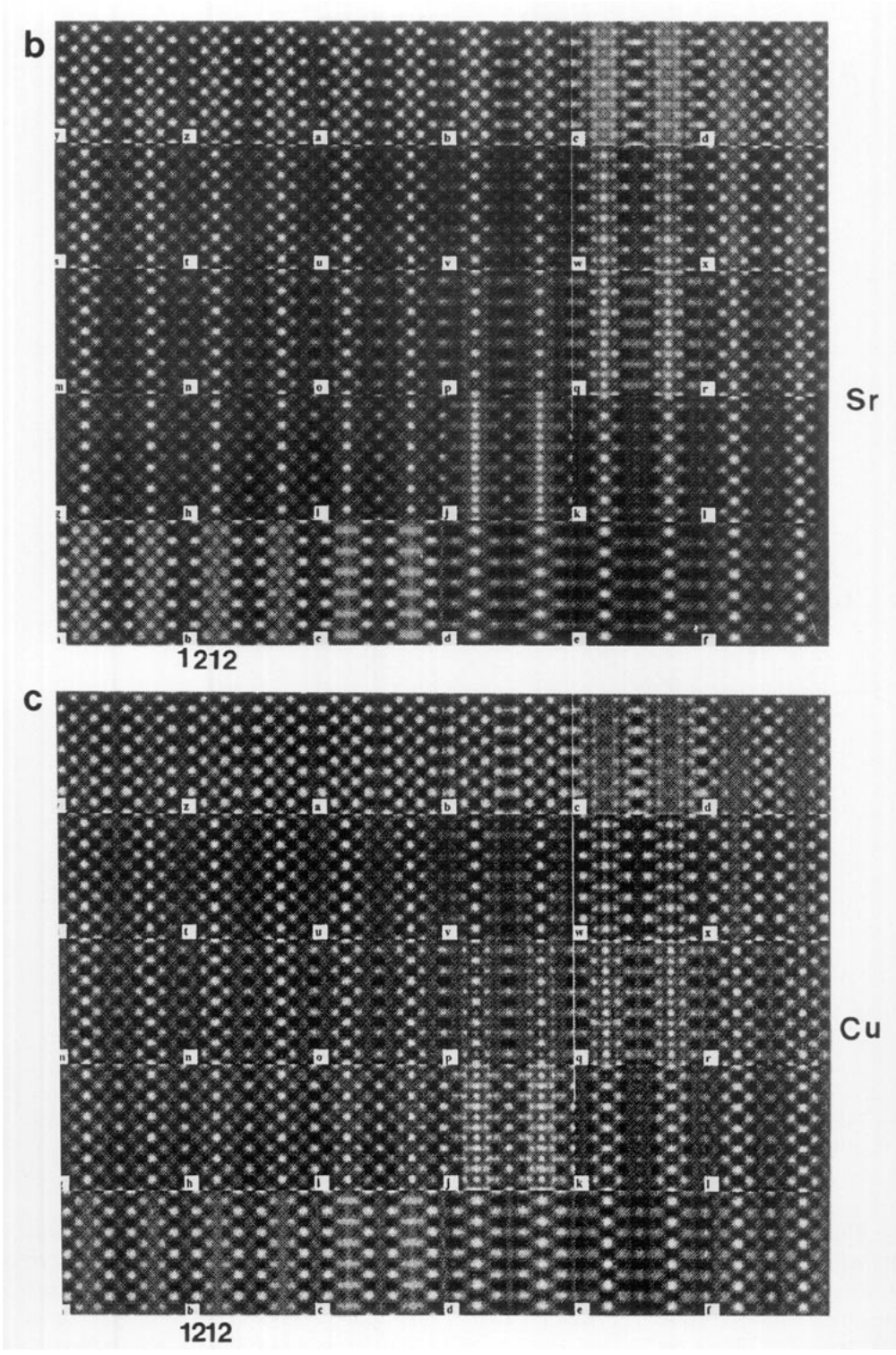

FIG. 8—*Continued*

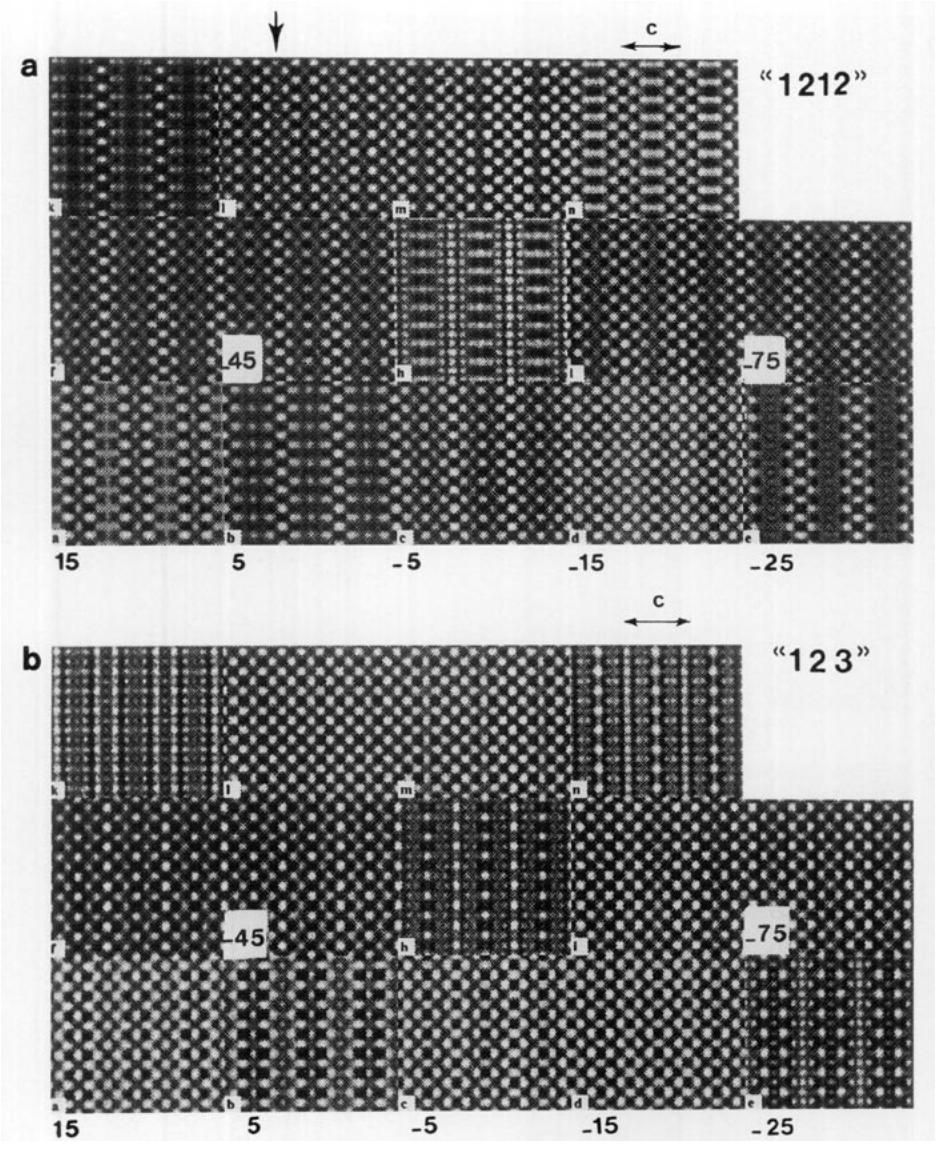

FIG. 9. Examples of calculated images for a) "1212" type structure: the intermediate layer is occupied by Sr in a rock salt layer, the positions of the atoms were calculated from usual interatomic distances. b) "123" type structure: the intermediate layer is a $[CuO_{2-\delta}]$ perovskite layer. The images are calculated from 15 to −115 nm (every 10 nm), the thickness is 3.1 nm.

11b). This type of defect can be compared to those observed in thallium oxides 2212 (*20*), where two additional $[CaO]_\infty$ layers are sometimes intercalated between two $[TlO]_\infty$ layers.

In the second example (Fig. 12a), it can be seen that the number of layers stacked along **c** remains constant but the contrast at the level of the intermediate layer (curved arrow) is considerably less intense than in the adjacent 1212 slices; simultaneously, a slight expansion of the *c* parameter is observed. Both features suggest that a layer "P" is locally replaced by a $[SrO]_\infty$ layer; it

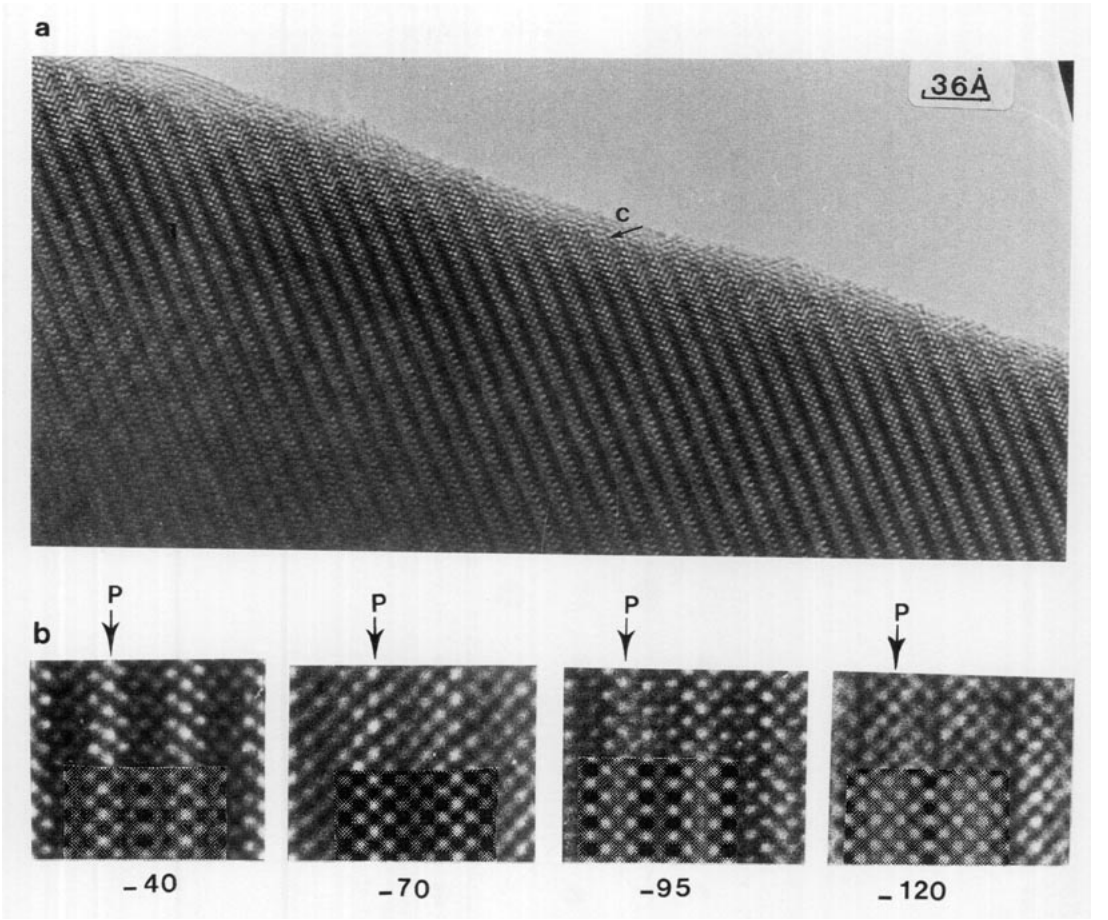

FIG. 10. $Pb_{0.5}Sr_{2.5}Y_{0.5}Ca_{0.5}Cu_2O_{7-\delta}$, [100] HREM images. a) Overall image showing the regular contrast observed in large areas. b) Comparison between the experimental images and the calculated images for a statistical distribution of the cations. The focus values are given in nm.

can be seen that, at the level of the defective slice, the contrast is similar to that calculated for $Sr_3YCu_2O_{7-\delta}$ (Fig. 9a). In this way, the 1212 type structure is locally retained but the composition is modified, with the sequence $[SrO]_\infty$ $[SrO]_\infty$ $[SrO]_\infty$ (Fig. 12b). It should be noted that the existence of triple $[SrO]_\infty$ adjacent layers have been observed, in the same way, as defects in the oxides $Sr_2NdCu_2O_{6-\delta}$ (*20*).

The third example (Fig. 13a) deals also with a variation in the layer composition but differs from the previous one by the fact that the nature of the cations is abruptly modified in the layer, involving the connection of two different structural types. In this image, the bright dots are correlated with the cationic positions; the nature of the different layers, in the normal contrast, is indicated on the right side of the image. On the left side, it can be seen that the three rows of white dots, correlated to $[SrO]_\infty$, $[P]_\infty$, and $[SrO]_\infty$ layers, respectively, are replaced by a row of weak dots intercalated between two rows of intense dots; simultaneously, a slight contraction of the *c* parameter is observed. This suggests that the three layers $[SrO]_\infty$ [P] $[SrO]_\infty$ of the 1212 structure have been replaced by three $[P]_\infty$ $[CuO_x]_\infty$ $[P]_\infty$ layers corresponding to a perovskite slab (Fig. 13b); this defect corresponds to

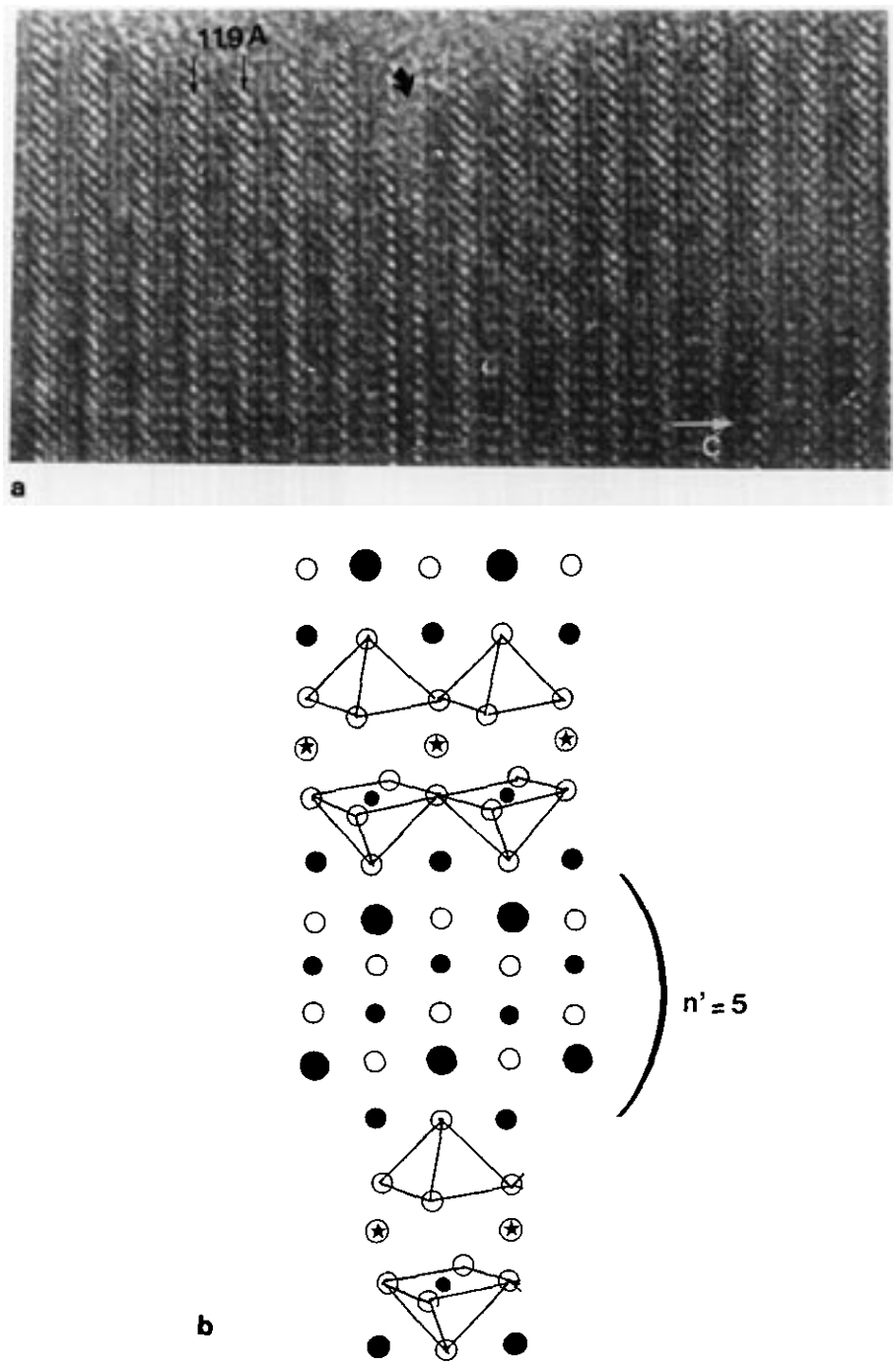

FIG. 11. "$Pb_{0.5}Sr_{0.5}$" a) the curved arrow shows the intercalation of two additional $[(Sr, Ca)O]_x$ leading to the formation of a $n' = 5$ defective member b) idealized model of the defect.

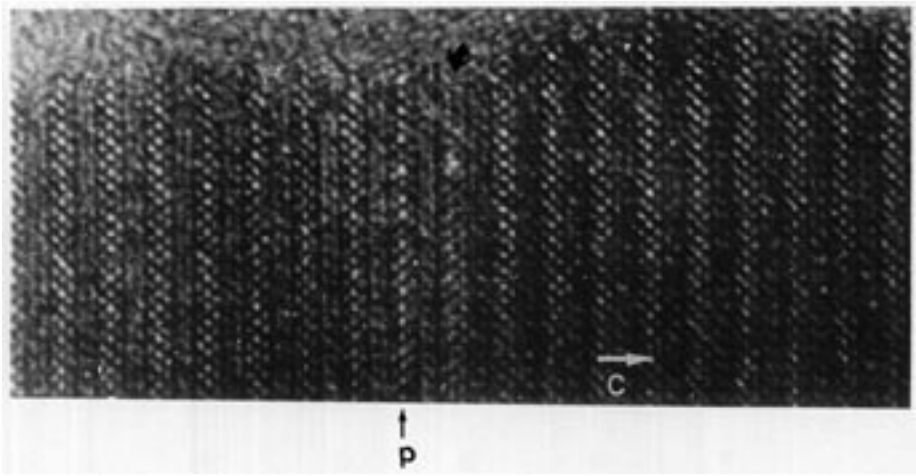

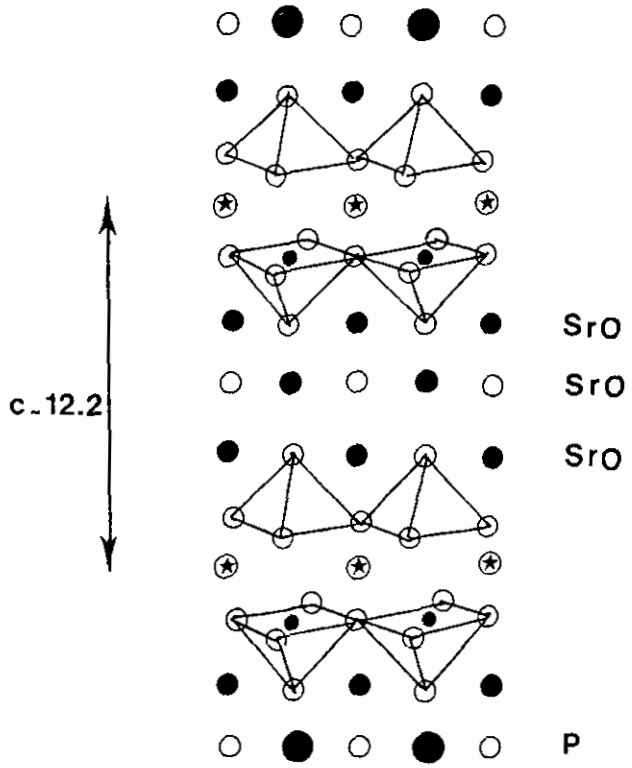

FIG. 12. "$Pb_{0.5}Sr_{0.5}$" a) the curved arrow shows a strong variation of the intensity at the level of the *P* layer and the parameter *c* increases locally. b) Idealized drawing of the defect corresponding to a sequence of three adjacent $[SrO]_\infty$ layers.

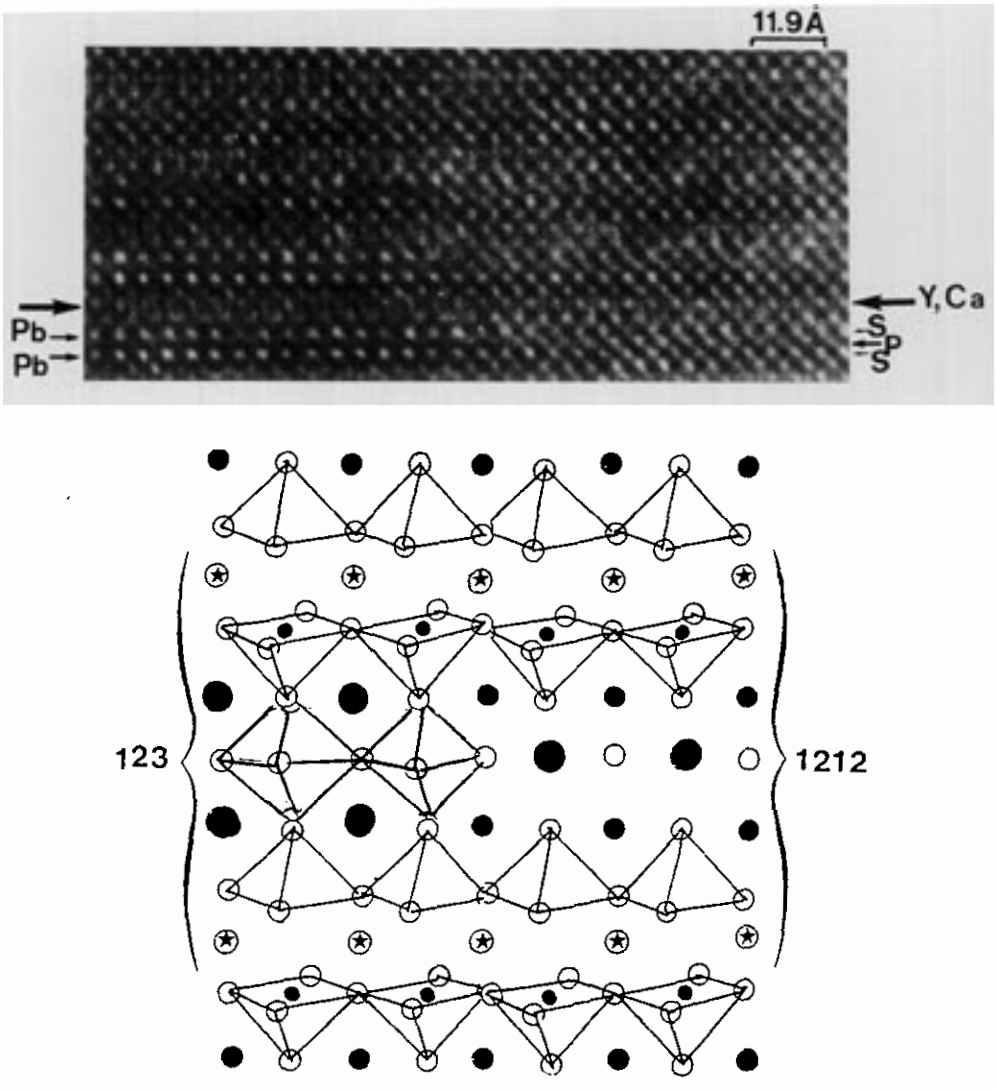

FIG. 13. "$Pb_{0.5}Sr_{0.5}$": a) variation of the contrast suggesting a connection between a "1212" and a "123"-type structure b) idealized model.

a junction of "1212"-type structure with "123" type structure.

The observation of the two latter defects is of importance since they correspond to the two extreme structural hypotheses which were considered as possible solutions for the mixed intermediate layer "P." In that way, it confirms first that the contrast is really different for these two structural arrangements, in agreement with our calculated images, and second, owing to the very few number of events which were observed, it shows that the eventuality of coexistence of two types of layers in the $Pb_{1-x}Sr_xSr_2Ca_{0.5}Y_{0.5}Cu_2O_{7-\delta}$ can be ruled out.

The modulated zones. As mentioned in the electron diffraction section, the existence of satellites in [100] E.D. patterns is an almost frequent phenomenon, whose intensity varies from one crystal to the other.

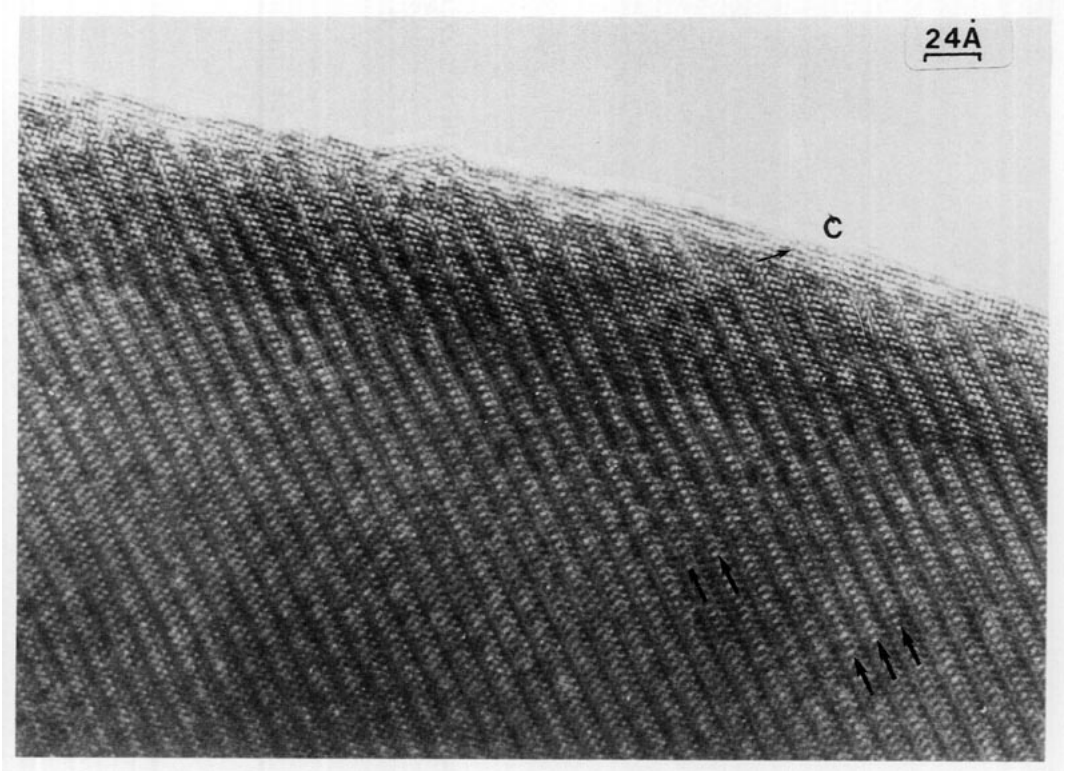

FIG. 14. Example of a large modulated area.

The corresponding images show that they are systematically associated with areas where the contrast is modulated, the surface of which is directly related to the intensity of the satellites. One example of a large modulated area is shown in Fig. 14, where the "P" layers are observed as the brightest rows (some are arrowed). In the thicker part of the crystal, although the contrast cannot be directly interpreted, it appears clearly that the "P" layers are not strongly affected by the modulations, contrary to the slice $[Sr_2Y_{0.5}Ca_{0.5}Cu_2O_6]_\infty$. The second example is shown in Fig. 15 for two focus values, $\Delta f \sim -700$ Å and $\Delta f \sim -1200$ Å where "P" layers and $[Y_{0.5}Ca_{0.5}]_\infty$ layers (labeled Y) are highlighted, respectively. The modulation is observed in a small area (right side of the images): it can be seen that the contrast at the level of the "P" layers (Fig. 15a) is considerably less modified than at the level of the perovskite slice. In some places, a regular variation of the contrast is observed, along **b**, with a new periodicity $4 \times a_p$ (Fig. 16a). These variations of the contrast may be correlated to Sr/Y/Ca and O/vacancies orderings; they can be compared with those observed in $Sr_2NdCu_2O_{5.66}$ oxides (*20*) which exhibit a superstructure $3 \times a_p$. Such an ordering would indeed imply significant displacements of the atoms. A theoretical model is proposed in Fig. 16b, based on a structural mechanism deduced from $Sr_2Nd\ Cu_2O_{5.66}$ and based on a $4 \times a_p$ superstructure. This model involves an oxygen deficiency which is compensated by an oxygen rearrangement and by partial occupancy of the oxygen sites of the "Y" layer (theoretically oxygen free); it corresponds to the formation of CuO_5 pyramids with basal planes perpendicular to the layers coupled with a possible Sr/Y exchange

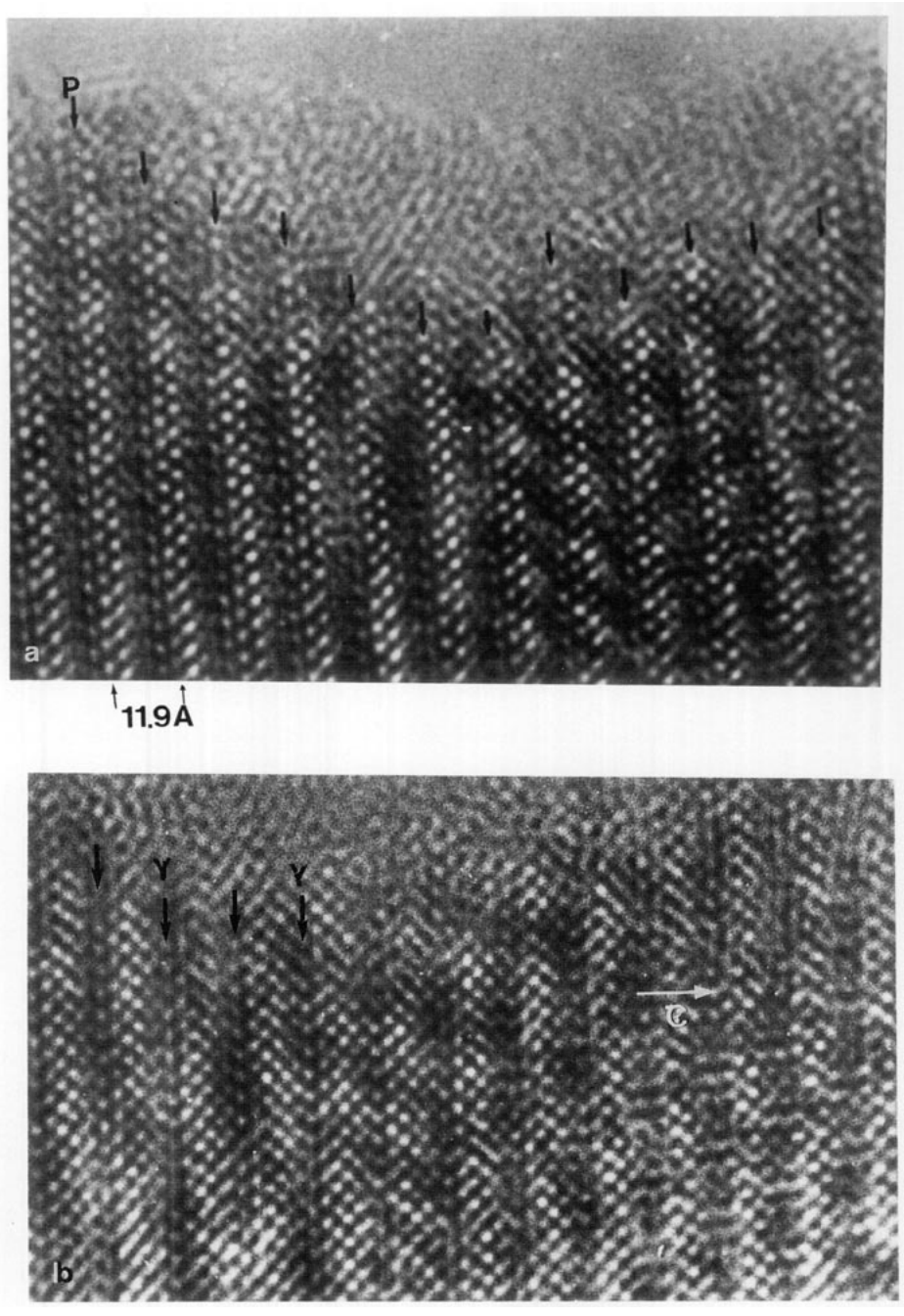

FIG. 15. Images of a small modulated area for a) −70 nm and b) −120 nm focus values.

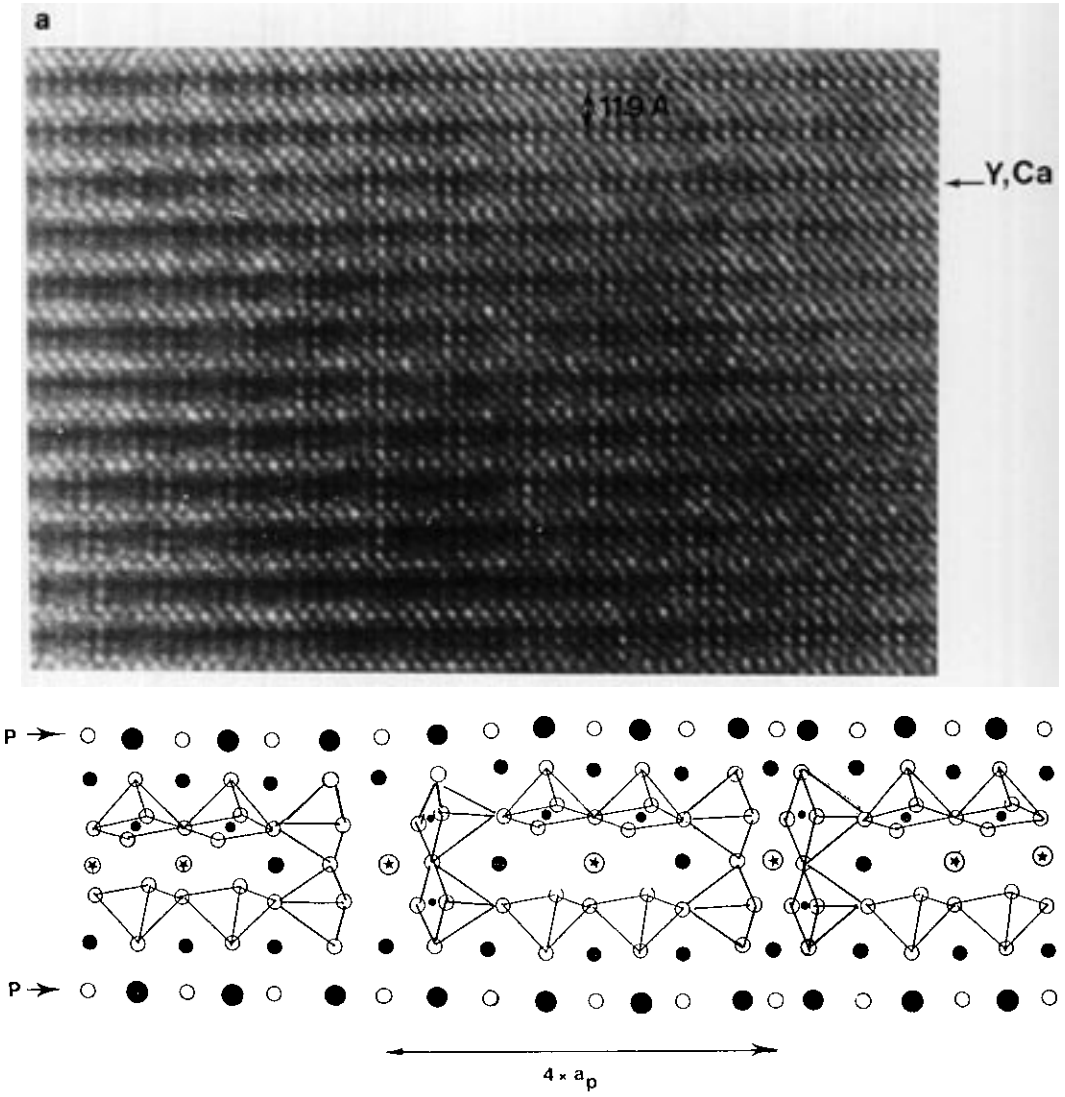

FIG. 16. a) Example of a local superstructure $4a_p$ in the $Pb_{0.5}Sr_{0.5}$ b) idealized model of the superstructure.

and a strong variation of the atomic positions.

Thus, the satellites which are observed in the E.D. patterns and the corresponding modulated areas arise mainly from atomic rearrangements in the $[Sr_2Y_{0.5}Ca_{0.5}Cu_2O_6]_\infty$ perovskite-type slices.

Local superstructures. Another type of atomic rearrangement is observed but, in contrast to the previous phenomena, the [100] images show that they affect especially the "P" and $[SrO]_\infty$ adjacent layers; moreover, they are always limited to small areas whose width is less than 100 Å. This is illustrated in Figs. 17 and 18. In the first example, the phenomenon is shown for two focus values, $\Delta f \sim -1200$ and -700 Å, in Fig. 17a and b respectively. A modulation of the contrast is clearly observed at the level of the three $[AO]_\infty$ adjacent layers where two

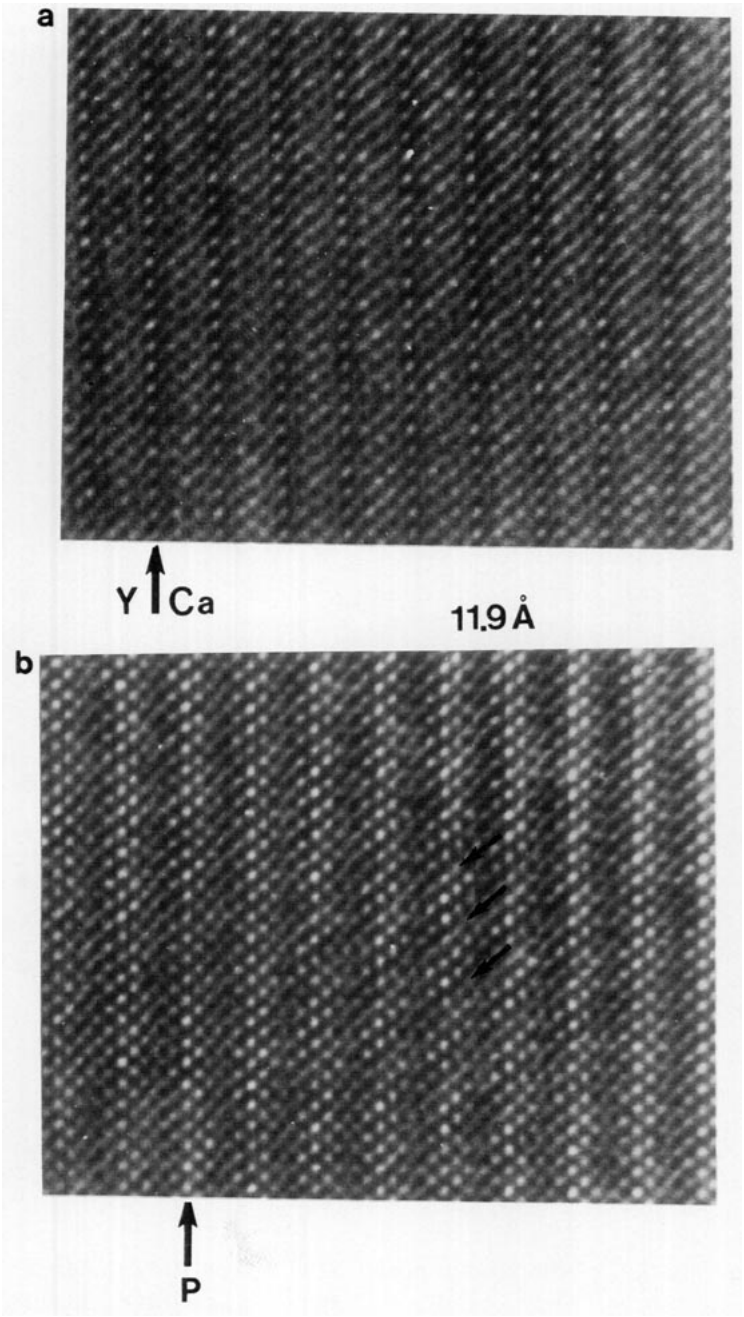

FIG. 17. Image of contrast variations at the level of the *P* layer a) −120 nm b) −70 nm.

rows of bright dots alternate with one row of weak dots along a direction which is roughly parallel to ⟨011⟩ (arrowed in Fig. 17b); the contrast at the level of the $[CuO_2]_\infty$ and [Y, $CaO]_\infty$ layers is not modified in most of these features. This type of modulation is to be compared to those described in the thallium deficient 2212 cuprates (*21*). They are, in

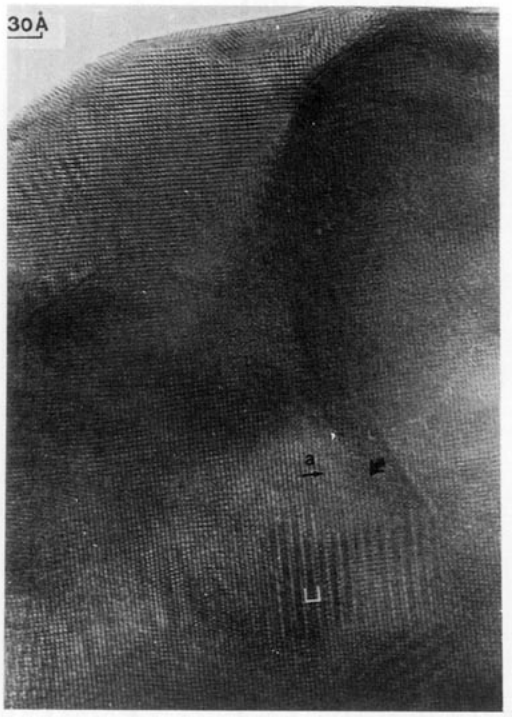

FIG. 18. [001] image of the "$Pb_{0.5}Sr_{0.5}$" showing local superstructures.

fact, observed in planes which are parallel to the (111) planes of the rock salt structure and could be correlated to a local lead–oxygen deficiency and a local ordering of the ions and vacancies. The [001] images give, in the same way, evidence of local superstructures which correspond generally to a doubling or to a tripling of the parameter a_p; owing to the common projection of the different types of atoms on the (001) plane, it is not possible to reach a direct correlation between the images and the structure. However, two points can be deduced from these observations. First, they are almost rare events, and second, they are always limited to small areas in the crystals. An example of $3 \times a_p$ local superstructure, viewed along [001] is shown in Fig. 18.

The crystal edges. Owing to the importance of the phenomenon on the resistivity measurements, it must be mentioned that amorphous films and/or crystallized microparticles are observed at numerous crystal edges. The thickness of the outfilms is generally of some nanometers and they consist of ill crystallized areas and $SrCO_3$ microcrystals.

$Pb_{0.7}Cu_{0.3}Sr_2Y_{0.85}Ca_{0.15}Cu_2O_7$

The characterization of the microstructural state of $Pb_{0.7}Cu_{0.3}Sr_2Y_{0.85}Ca_{0.15}Cu_2O_7$ samples by HREM appeared very difficult because the contrast is generally too disturbed to allow a direct interpretation. In some crystals, however, regular zones were observed; in that case, the images exhibit a contrast which is similar to that recorded for the "$Pb_{0.5}Sr_{0.5}$" sample. An example of such an area is presented in Fig. 19a; in the enlarged image (Fig. 19b) the contrast can be compared to that of the calculated images in Fig. 8.

All the crystals exhibit a great regularity of the stacking of the layers along the **c** axis. The most striking features is the speckled aspect of the crystals; two examples are given in Fig. 20a and b for a [001] and [100] orientation respectively. An enlarged image of the [001] plane (Fig. 20c) shows that this aspect is due to modulations of the contrast along one or two directions. These modulations are correlated with the streaks and extra spots observed in the [001] E.D. patterns (Fig. 7). The high resolution images show that in fact few zones exhibit a regular contrast (white triangle in Fig. 20d); superstructures with $n \times a_p$ (n = 2 to 5) (Fig. 20c) and modulations and moiré patterns resulting from the superposition of these phenomena (Fig. 20d) are the common features of the $Pb_{0.7}Cu_{0.3}$ sample. Similar observations were made along [100].

Owing to the complexity of the structural features which take place in the $Pb_{0.7}Cu_{0.3}$ samples it is unreasonable to propose structural models. The magnitude and the systematical occurrence of the phenomena suggest that they are correlated to local cationic

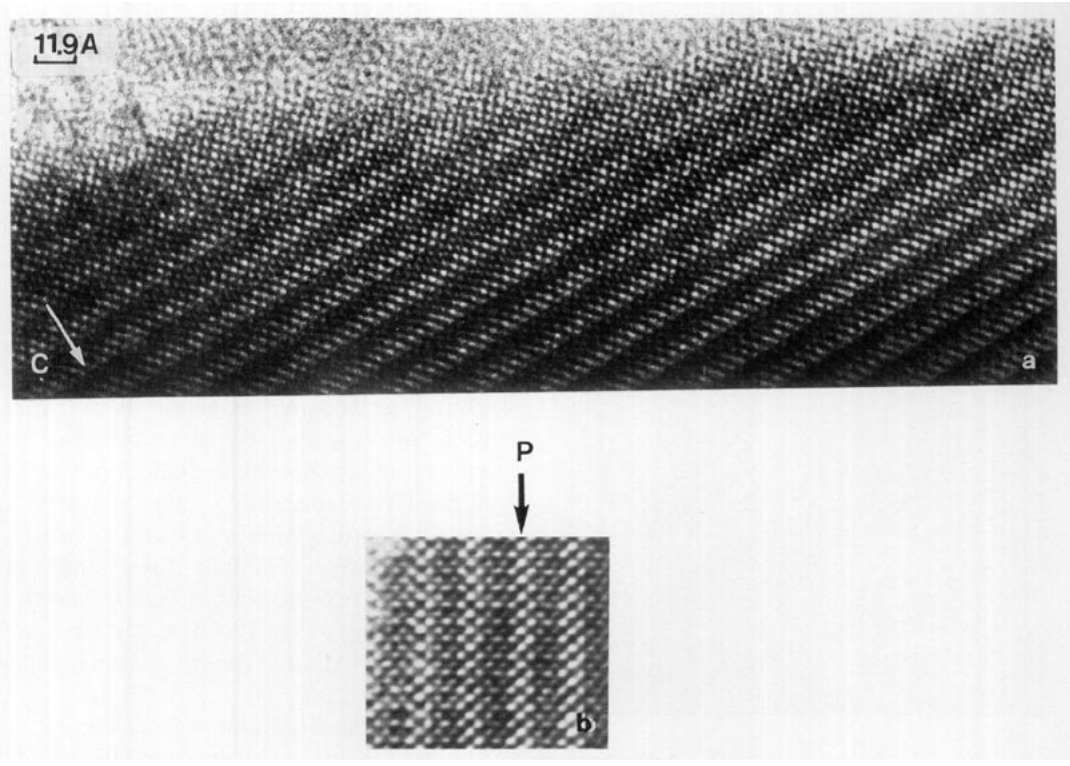

FIG. 19. a) one of the rare zones of regular contrast observed in "$Pb_{0.7}Cu_{0.3}$" b) the enlargement shows that the contrast is similar to that calculated in Figure 8a.

arrangements coupled with strong displacements and cell distortions.

Concluding Remarks

If the X-ray diffraction patterns of the lead cuprates with nominal compositions $Pb_{0.5}Sr_{0.5}Sr_2Y_{0.5}Ca_{0.5}Cu_2O_{7-\delta}$ and $Pb_{0.7}Cu_{0.3}Sr_2Y_{0.85}Ca_{0.15}Cu_2O_{7-\delta}$ exhibit great similarities, the electron diffraction and electron microscopy studies give evidence of highly different microstructural states for the two compounds. From E.D. characterization, the subcells indeed appear similar and from the HREM study, the layer stacking in the regular zones is that of a 1212 structural type for the two oxides. In fact, they differ by the nature, the frequency, and the magnitude of the order–disorder phenomena which are responsible for the extra sptos, satellites, and diffuse streaks in the E.D. patterns. These features are most dominant in the ($Pb_{0.7}Cu_{0.3}$) sample where they generally occur at short distances and in the form of small adjacent domains. They suggest a fundamental inhomogeneity of the distribution of the atoms in the matrix; it would be important to check their evolution under different thermal treatments and annealings.

In contrast, the large zones of regular contrast observed in the ($Pb_{0.5}Sr_{0.5}$) sample confirm that a statistical distribution of the cations (and vacancies) is ensured in the intermediate layer P. The modulated zones are correlated to order–disorder phenomena in the perovskite slices, similar to those observed in the $Sr_2NdCu_2O_{5.66}$ oxides (*20*) which can be correlated to local variations of the oxygen content; their disappearance by annealing is in agreement with such a hypothesis.

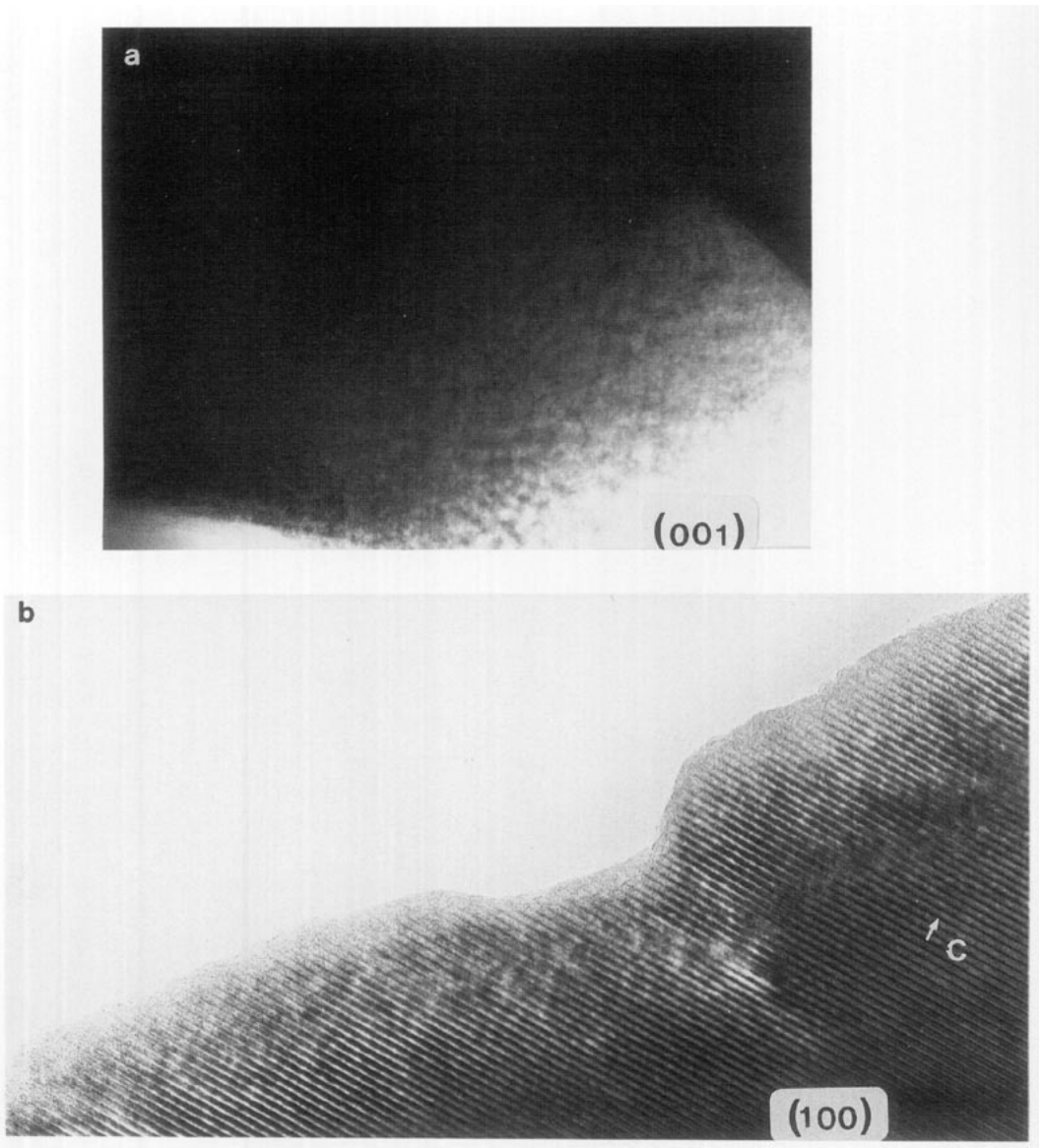

FIG. 20. The crystals of "$Pb_{0.7}Cu_{0.3}$" exhibit a speckel contrast as well along [001] (a) as along [100] (b). The enlargement gives evidence of local modulations (c) and superstructures (d) which are often superposed.

These results are of interest for the understanding of the superconducting properties of these materials. They demonstrate the inhomogeneity of the distribution of cations, oxygens, and vacancies at the level of the mixed $[Pb_{1-y}A_yO]_\infty$ rock salt layers but also at the level of the $[Y, Ca]_\infty$ layers between the pyramidal copper layers. Such local ordering is in agreement with the broad transition observed on the magnetic susceptibility curves $\chi'(T)$ for these oxides.

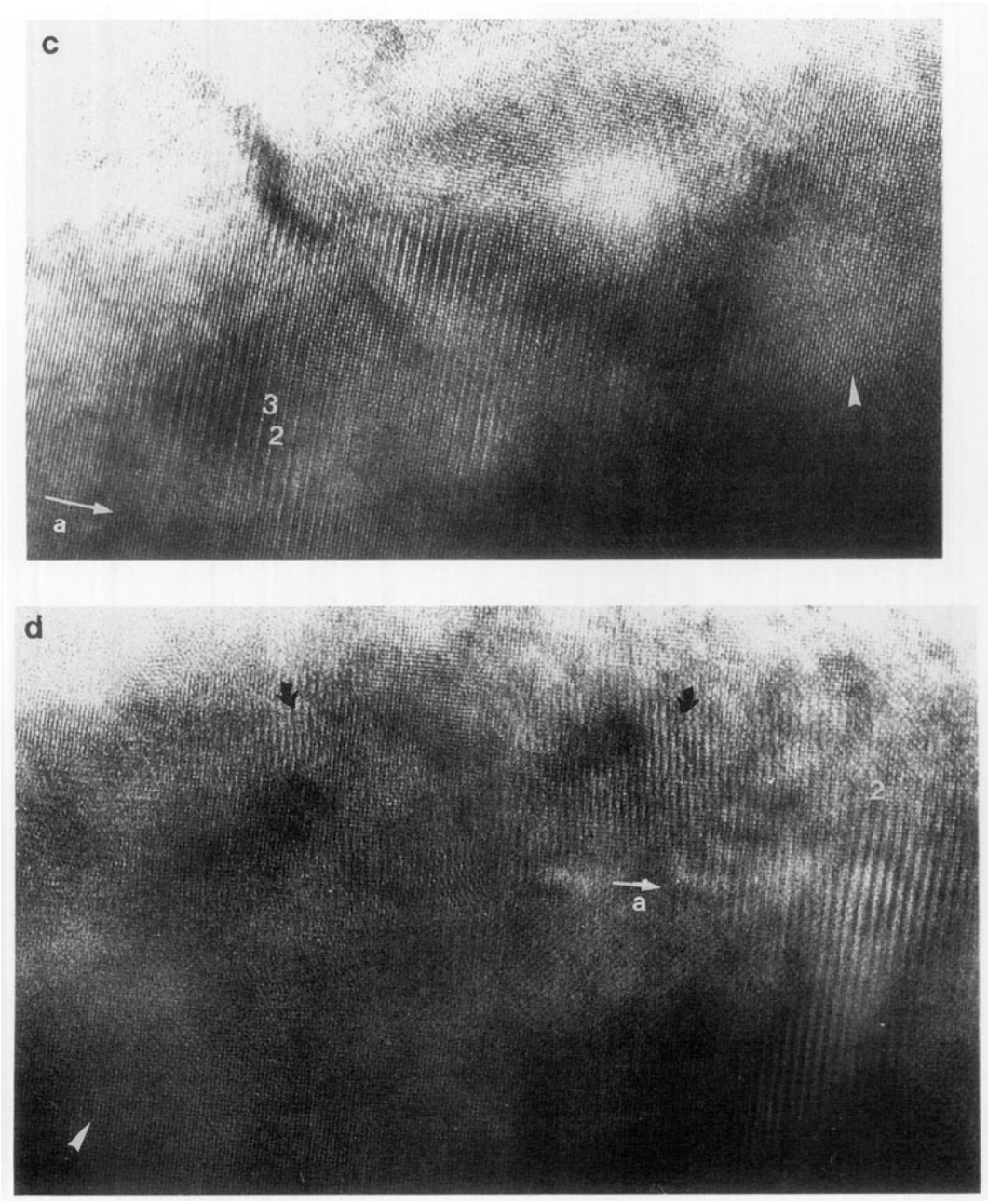

FIG. 20—*Continued*

References

1. T. ROUILLON, J. PROVOST, M. HERVIEU, D. GROULT, C. MICHEL, AND B. RAVEAU, *Physica C* **159,** 209 (1989).
2. T. ROUILLON, J. PROVOST, M. HERVIEU, D. GROULT, C. MICHEL, AND B. RAVEAU, *J. Solid State Chem.* **84,** 375 (1990).
3. T. ROUILLON, A. MAIGNAN, M. HERVIEU, C. MICHEL, D. GROULT, AND B. RAVEAU, *Physica C* **171,** 7 (1990).
4. M. A. SUBRAMANIAN, J. GOPALAKRISHNAN, C. C.

TORARDI, P. L. GAI, E. D. BOYES, T. R. ASKEW, R. B. FLIPPEN, W. E. FARNETH, AND A. W. SLEIGHT, *Physica C* **157,** 124 (1989).
5. J. Y. LEE, J. S. SWINNEA, AND H. STEINFINK, *J. Mater. Res.* **4**(4), 763 (1989).
6. T. MAEDA, K. SAKUYAMA, F. IZUMI, H. YAMAUCHI, H. ASANO, AND S. TANAKA, *Physica C* **175,** 393 (1991).
7. J. Y. LEE, J. S. KIM, J. S. SWINNEA, AND H. STEINFINK, *J. Solid State Chem.* **84,** 335 (1990).
8. A. ONO AND Y. UCHIDA, *Jpn. J. Appl. Phys.* **29**(4), L586 (1990).
9. T. MAEDA, K. SAKUYAMA, S. KORIYAMA, H. YAMAUCHI, AND S. TANAKA, *Phys. Rev. B* **43**(10), 7866 (1991).
10. S. ADACHI, H. ADACHI, K. SETSUNE, AND K. WASA, *Jpn. J. Appl. Phys.* **30**(4B), L690 (1991).
11. R. S. LIU, S. F. HU, I. GAMSON, P. EDWARDS, A. MAIGNAN, T. ROUILLON, D. GROULT, AND B. RAVEAU, *J. Solid State Chem.* **93,** 276 (1991).
12. R. S. LIU, P. T. WU, S. F. WU, W. N. WANG, AND P. P. EDWARDS, *Physica C* **165,** 111 (1990).
13. R. S. LIU, P. P. EDWARDS, AND P. T. WU, *Advanced Mater.* **2**(8), 369 (1990).
14. S. CLAUDE, M. HERVIEU, AND P. T. MOSELEY, *J. Mater. Chem.* **4,** 471 (1992).
15. R. S. LIU, S. F. HU, AND P. P. EDWARDS, *Appl. Phys. Lett.* **59,** 985 (1991).
16. R. S. LIU, D. GROULT, A. MAIGNAN, S. F. HU, D. A. JEFFERSON, B. RAVEAU, C. MICHEL, M. HERVIEU, AND P. P. EDWARDS, *Physica C* **195,** 35 (1992).
17. A. MAIGNAN, D. GROULT, R. S. LIU, T. ROUILLON, P. DANIEL, C. MICHEL, M. HERVIEU, AND B. RAVEAU, *J. of Solid State Chem.*, in press.
18. B. RAVEAU, C. MICHEL, M. HERVIEU, AND D. GROULT, "CRYSTAL CHEMISTRY OF HIGH T_c Superconducting Copper Oxides," Springer-Verlag, Berlin/New York (1991).
19. P. A. STADELMANN, *Ultramicroscopy* **21,** 131 (1987).
20. M. HERVIEU, V. CAIGNAERT, C. MICHEL, R. RETOUX, AND B. RAVEAU, *Microsc. Microanal. Microstruct.* **1,** 109 (1990).
21. C. MICHEL, C. MARTIN, M. HERVIEU, A. MAIGNAN, J. PROVOST, M. HUVÉ, AND B. RAVEAU, *J. Solid State Chem.* **96,** 271 (1992).